Journal of Materials Chemistry B

PAPER

View Article Online
View Journal | View Issue

Cite this: J. Mater. Chem. B, 2014, 2, 4876

A multiwalled carbon nanotube/tetra-β-isoheptyloxyphthalocyanine cobalt(II) composite with high dispersibility for electrochemical detection of ascorbic acid†

Miao Shi,[a] Zhimin Chen,*[a] Liangxiao Guo,[a] Xiuhua Liang,[a] Jialin Zhang,[a] Chunying He,[a] Bin Wang[a] and Yiqun Wu[ab]

Received 11th February 2014
Accepted 22nd May 2014

DOI: 10.1039/c4tb00229f

www.rsc.org/MaterialsB

A sensitive electrochemical sensor for ascorbic acid (AA) is designed and synthesized *via* the following steps. The novel tetra-β-isoheptyloxyphthalocyanine cobalt(II) (PcCo) spontaneously adsorbs on the surface of acid-treated multi-walled carbon nanotubes (aMWCNTs). Then, the aMWCNT/PcCo composite was immobilized on the glassy carbon electrode (GCE). The results of UV-vis, FT-IR, TG, XPS, SEM and TEM revealed the successful self-assembly between PcCo and aMWCNTs *via* the π–π stacking interaction, and the aMWCNT/PcCo composite appears to have a uniform network-like structure on the GCE surface due to the four peripheral isoheptyl substituents of PcCo. Such a structure can effectively increase the electrode area, facilitate the mass transport of analytes and provide continuous conducting pathways for the transportation of electrons. Synchronously, benefitting from the synergistic effect between PcCo and aMWCNTs, the obtained electrochemical sensor has a high current and low potential for the oxidation of AA. The linear range for the AA detection is from 10 μM to 1.2 mM and the detection limit is as low as 4.0 μM. The developed biosensor exhibited good reproducibility and acceptable stability, providing a simple method for the analysis of AA.

1. Introduction

Ascorbic acid (AA), also known as vitamin C, is an essential nutrient for humans and plays an important role in helping the immune system, joints and arteries heal and function properly.[1] A deficiency of AA can lead to scurvy, which causes muscle weakness, swollen and bleeding gums, and bleeding under the skin, as well as tiredness and depression. In contrast, an excess of AA can cause diarrhea, insomnia and kidney stones.[2] Thus, a reliable, accurate, sensitive, rapid, and low-cost determination of AA is important in a variety of areas such as foods, drugs, and industrial applications. Among various analytical techniques, the electrochemical sensing of AA is especially attractive due to its simplicity, cost-effectiveness, fast response, high sensitivity, and ease of miniaturization.[3–6] However, the direct determination of AA with plain electrodes, such as carbon and metallic electrodes, generally suffers from a large overpotential and poor selectivity in the presence of interfering compounds.[4–8] Thus, it is important to develop an efficient electrocatalyst for chemically modified electrodes (CMEs), which can offer high sensitivity and selectivity at a lower operating potential for the detection of AA.

Carbon nanotubes (CNTs), a unique quasi-one-dimensional nanostructure material, have captured worldwide interest due to their huge surface area, abundant microchannel porous structure, high electrical conductivity, electron transfer rate and excellent thermal stability.[9–12] Thus, CNTs are a good kind of electrocatalysts and electrode modifying materials, which have been reported widely.[13–18] However, due to the strong van der Waals attraction, CNTs tend to restack or aggregate both in solution and in the solid state, forming bundled structures that significantly reduce the active surface area, greatly hinder mass transport in the electrochemical process and often cause low reproducibility of the electrocatalysis properties. One of the effective strategies to enhance the dispersion of CNTs is the surface modification of CNTs *via* covalent or noncovalent.[19–24] In particular, the latter has the advantage of preserving the electronic structure of CNTs and therefore their transport and surface properties.[25–28]

Metal phthalocyanines (MPcs), a well-known class of planar two-dimensional metal complexes with conjugated delocalized 18π-electron systems, have a great versatility due to their

[a]Key Laboratory of Functional Inorganic Material Chemistry (Ministry of Education of China), School of Chemistry and Materials Science, Heilongjiang University, Harbin 150080, People's Republic of China. E-mail: zmchen@siom.ac.cn; Fax: +86 451 8660 9145; Tel: +86 451 8660 9145

[b]Shanghai Institutes of Optics and Fine Mechanics, Chinese Academy of Sciences, Shanghai 201800, People's Republic of, China

† Electronic supplementary information (ESI) available: Other detailed characterization. See DOI: 10.1039/c4tb00229f

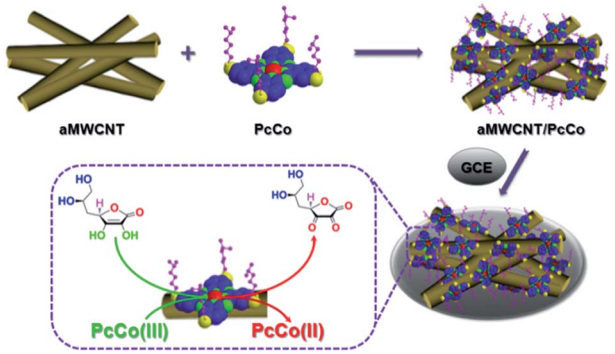

Scheme 1 Schematic representation of the fabrication and electroanalysis mechanism of aMWCNT/PcCo-modified electrodes for AA.

electrochemical activity as electrocatalysts.[29–35] However, when MPcs are used as modifiers for voltammetric electrodes, the unfavourable electroanalysis signals are commonly produced due to their poor conductivity. Further, the bonding of MPcs to the electrode is neither reproducible nor long-term stable. Recent studies have shown that CNT/MPc modified electrodes can bring a notable improvement to the electrocatalytic properties, in comparison with the free CNTs or MPcs.[36–45] Nevertheless, the very poor solubility of most reported cases, in which the substituents of MPcs are extremely limited to amino-,[46–50] sulfo-,[51–53] and unsubstituents,[39–45] often precludes the study of their electrocatalyst properties.

Based upon the consideration of the above requirements, we design and synthesize a new phthalocyanine, tetra-β-isoheptyloxyphthalocyanine cobalt(II) (PcCo), which has four long-alkyl chains at peripheral positions, leading to high solubility in various organic solvents. PcCo can further spontaneously assemble with CNTs *via* noncovalent. The obtained composite combines the excellent dispersibility and Co(II)/(III) redox of PcCo with the outstanding electronic properties of MWCNTs by π–π stacking PcCo to CNTs, resulting in the excellent electrocatalytic activity of AA, as shown in Scheme 1. As far as we are aware, this is the first report of combining long-alkyl chain substituted MPcs with CNTs to construct CMEs for the detection of AA.

2. Experimental

2.1. Reagents

Multiwalled carbon nanotubes (MWCNTs) (>95%) were purchased from Shenzhen Nanotech Port Co. Ltd. (Shenzhen, China). Before use, MWCNTs were treated with concentrated acids (H_2SO_4–HNO_3 in 3 : 1 v/v ratio) in the presence of ultrasonication at 80 °C for 10 h. The acid-treated MWCNTs (aMWCNT) were washed with copious of water and then dried at 60 °C. Tetra-β-isoheptyloxyphthalocyanine cobalt(II) (PcCo) was synthesized by the template-reaction method in the presence of 1,8-diazabicyclo[5,4,0]undec-7-ene (DBU) (see ESI† for experimental details). Nafion (5% (w/w) in low aliphatic alcohols and water) was purchased from Sigma-Aldrich Co. LLC. Ultrapure water of resistivity 18.2 MΩ cm was obtained using a Milli-Q Water System (Millipore Corp. Bedford, MA, USA) and was used throughout for the preparation of solutions. Phosphate buffer solutions (PBS, 0.1 M, pH = 7.0) were prepared by mixing standard stock solutions of Na_2HPO_4 and NaH_2PO_4. All other reagents were of analytical grade and were used as received from the suppliers without further purification.

2.2. Preparation of the aMWCNT/PcCo composite

The aMWCNT/PcCo composites, well-dispersed in some common solvents, were synthesized through the π–π stacking interaction between aMWCNTs and PcCo (Scheme 1). In a typical experiment, aMWCNTs (20 mg) were added to dry DMF (20 mL) in a 50 mL round-bottomed flask. The resulting solution was sonicated in an ultrasonic bath for 1 h. PcCo (80 mg) was then added and the reaction mixture was stirred at room temperature under N_2 for 3 days. After the reaction was finished, the resultant solution was filtered through a 0.22 μm PTFE membrane. The filter cake on the Millipore film was collected and washed with ethanol, acetone, dichloromethane and tetrahydrofuran for several times, successively, after which the filtrate became colorless, and then dried at 50 °C for 1 h, affording the desired aMWCNT/PcCo composite as black powders.

2.3. Preparation of modified glassy carbon electrodes (GCEs)

The GCEs (diameter: 3 mm, CHI) were carefully polished to a mirror-like plane with 0.3, 0.1, and 0.05 μm alumina powders, successively, and then sonicated in pure water and absolute ethanol for 2 min, respectively, and dried at room temperature. The as-prepared aMWCNT/PcCo composite (2 mg) and 5% (w/w) Nafion (80 μL) were dispersed in absolute ethanol (1 mL) to obtain a uniform suspension of 2 mg mL^{-1} by ultrasonication for 20 min. The suspension was essentially stable. No precipitation or flocculation is observed even after 3 months. Then the aMWCNT/PcCo homogeneous suspension (2 μL) was spread evenly onto the well-polished GCE surface and allowed to dry at ambient temperature, denoted as aMWCNT/PcCo/GCE. For comparison, the PcCo/GCE and aMWCNT/GCE were also fabricated by the similar procedures.

2.4. Apparatus

UV-vis absorption spectra were recorded with a Lambda 35 UV-vis spectrometer (Perkin-Elmer, USA). FT-IR spectra were recorded on a Nicolet FT-IR NEXUS spectrometer (Thermo Scientific). Scanning electron microscopy (SEM) images were recorded with a Hitachi S-4800 field emission scanning electron microscope operating at 15 kV. Transmission electron microscopy (TEM) was performed on a JEM-3010 electron microscope (JEOL, Japan) with an acceleration voltage of 300 kV. X-ray photoelectron spectroscopy (XPS) measures were performed with an AXIS ULTRA DLD. Thermogravimetric (TG) analysis was performed on a TA Q600 under a stream of nitrogen at a heating rate of 10 °C min^{-1}. Electrochemical measurements were performed on a computer-controlled CHI660D electrochemical workstation (CH Instrument, Shanghai, China). All the electrochemical measurements were carried out in 0.1 mol L^{-1} PBS

at room temperature (25 ± 2 °C) using a conventional three-electrode system with a modified GCE as a working electrode, a platinum foil as an auxiliary electrode, and a saturated calomel electrode (SCE) as a reference electrode. All potentials in this study were reported with respect to the SCE. The electrolyte was purged with high purity nitrogen for at least 10 min prior to measurements to remove the dissolved oxygen unless otherwise stated.

3. Results and discussion

3.1. Characterization of the aMWCNT/PcCo composite

According to our design, due to the strong π–π interaction, PcCo can spontaneously assemble with aMWCNTs, giving the aMWCNT/PcCo composite,[25–28] which is confirmed by UV-vis spectra (as shown in Fig. 1A). The spectrum of PcCo in CH_2Cl_2 solutions shows typical electronic absorption spectra with two strong absorption regions, one in the UV region at about 328 nm (B-band) and the other in the visible region at 669 nm (Q-band) with a weaker satellite band around 605 nm, which is the characteristic of non-aggregated PcCo.[54–56] It could be attributed to the steric hindrance of peripheral long-chain alkyl substituents, which can effectively restrain the formation of dimers. Meanwhile, different from aMWCNTs, the characteristic Q-band of PcCo is observed in the UV-vis spectrum of the aMWCNT/PcCo composite, indicating the successful self-assembly of PcCo on the surface of aMWCNTs. However, an obvious red shift about 9 nm for the Q-band appears in the spectrum of the aMWCNT/PcCo composite, originating from the charge transfer of the PcCo ring to aMWCNTs.[36,45,57] Fig. 1B shows the FT-IR spectra of aMWCNTs, PcCo and aMWCNT/PcCo. The results reveal that the characteristic bands of the carboxyl group on aMWCNTs appear at 1717 cm^{-1} (C=O stretching) and 3428 cm^{-1} (O–H stretching).[14,15] Compared with the FT-IR spectrum of the aMWNTs, the characteristic peaks of pure PcCo obviously appear in the spectrum of aMWCNT/PcCo. Of these bands, the absorption at 2959 cm^{-1} ($\nu_{as}CH_3$), 2929 cm^{-1} ($\nu_{as}CH_2$) and 2857 cm^{-1} (ν_sCH_3, CH_2) is attributed to peripheral isoheptyl groups of PcCo and the absorption around 1228 (ν_{as}C–O) and 1058 cm^{-1} (ν_sC–O) is assigned to the vibration of the Ar–O–alkyl bond, but other remaining bands observed near 1608 cm^{-1} (νC=N) and 1460 cm^{-1} (νC=C) would be mostly due to the various skeletal vibrations of the phthalocyanine ring.[41,45,46] The slight shift of these peaks compared to pure PcCo suggests that electron delocalization due to π–π interactions took place, further indicating the formation of the π–π bonded composite of aMWCNTs and PcCo.[48,50,57]

Further XPS was employed to characterize the surface chemical compositions and valence states of the aMWCNT/PcCo composite. The survey spectrum reveals the presence of C, N, O, and Co in the aMWCNT/PcCo composite (Fig. 2A). The Co 2p peaks of as-obtained aMWCNT/PcCo could be fitted to four contributors (Fig. 2B), corresponding to Co $2p_{1/2}$ at 796.8 eV, $2p_{3/2}$ at 781.3 eV, and two relatively weaker satellite features.[56–58] The content of the Co element at the aMWCNT/PcCo composite is measured to be about 0.35 at.% by XPS analysis. Meanwhile, the N 1s XPS spectrum splits into two peaks: aza-bridging nitrogen (399.0 eV) and pyrrole nitrogen (400.6 eV), respectively.[59] The XPS spectroscopy data show the chemical nature of PcCo, which further imply successful attachment of PcCo onto the surface of aMWCNTs.

The amount of PcCo assembled on aMWCNTs has been evaluated by TG analysis under a N_2 atmosphere (Fig. 2D). A loss of weight of about 18% for aMWCNTs between 100 and 800 °C can be observed, which ascribes to the destruction of the residual amorphous carbon and the decarboxylation of the oxidized species.[60] The TG curve of PcCo presents a loss of weight about 33.9% from 348 to 423 °C sharply, indicating the thermal decomposition of long-chain alkyl substituents in a N_2 atmosphere. Similar to PcCo, a greater weight loss of aMWCNT/PcCo also appears between 357 and 423 °C. Considering the weight loss of aMWCNTs, the corrected weight loss due to PcCo is then estimated to be 2.5%. Actually, concerning the amount of PcCo adsorbed on the surface of aMWCNTs, a real ratio of 7.4% (2.5%/33.9%) can be calculated, taking into account the weight loss of both PcCo and aMWCNTs. Such results further indicate that PcCo has adsorbed on aMWCNTs successfully *via* the π–π interaction.

The surface morphology and structure of the synthesized aMWCNT/PcCo composite were investigated by SEM and TEM,

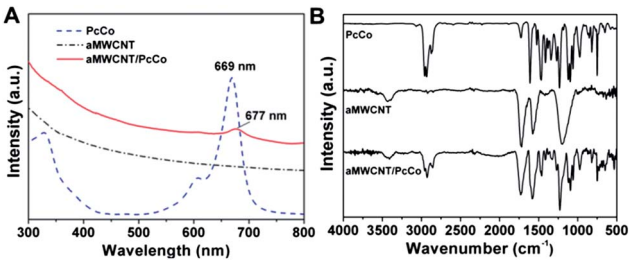

Fig. 1 UV-vis and FT-IR of aMWCNTs, PcCo, and aMWCNT/PcCo.

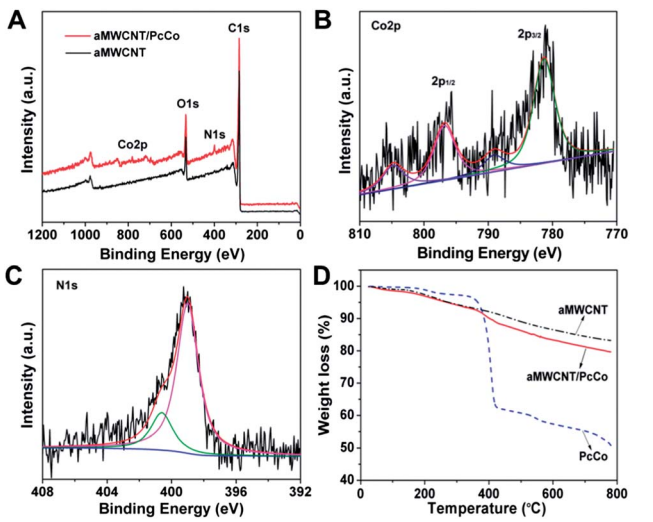

Fig. 2 (A) XPS spectra of aMWCNT/PcCo and aMWCNTs; (B and C) the high-resolution XPS spectrum of Co 2p and N 1s, respectively; (D) TGA profiles of aMWCNTs, PcCo, and aMWCNT/PcCo measured under a N_2 atmosphere.

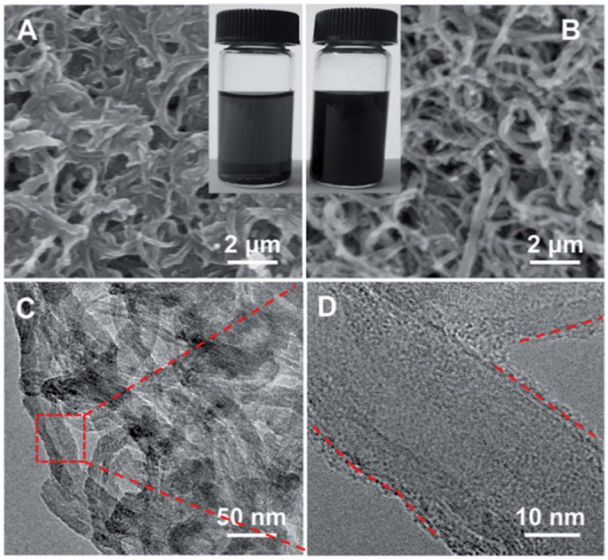

Fig. 3 (A) SEM image of aMWCNTs and (B–D) SEM and TEM images of aMWCNT/PcCo (inset images: the optical photographs of equivalent aMWCNTs and aMWCNT/PcCo dispersed in ethanol, respectively).

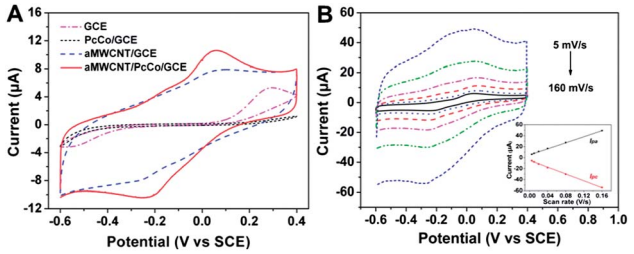

Fig. 4 (A) CVs of aMWCNT/PcCo/GCE, aMWCNT/GCE, PcCo/GCE, and bare GCE in 0.1 M PBS (pH = 7.0) containing 1.0 mM AA, scan rate: 10 mV s^{-1}; (B) CVs of aMWCNT/PcCo/GCE in 0.1 M PBS (pH = 7.0) containing 1.0 mM AA measured at different scan rates (5, 10, 20, 40, 80, and 160 mV s^{-1}). The inset image shows calibration plots between the anodic and cathodic peak currents and the scan rate (I_{pa} = 276.08V + 5.1868, R^2 = 0.9994 and I_{pc} = −312.05V − 4.7999, R^2 = 0.9984; I_{pa}, I_{pc}, and V are anodic, cathodic peak currents and scan rate, respectively).

as shown in Fig. 3. It is clear that both aMWCNTs and the aMWCNT/PcCo composite appear to have as the three-dimensionally network-like structure. Note that, different from the severe aggregation of aMWCNTs, the aMWCNT/PcCo composite becomes looser and individual nanotubes are clear, mainly due to the non-covalent modification of aMWCNTs by PcCo. Such a loose and interconnected structure not only effectively increases the electrode area but also facilitates the mass transport of analytes.[16,36,57] Synchronously, it may also provide continuous conducting pathways for the transportation of electrons, which is beneficial for increasing the sensitivity of electrochemical response.[36] In addition, due to the assembly of aMWCNTs and PcCo, the dispersion of the aMWCNT/PcCo composite in ethanol has improved dramatically. The black and uniform solution of the aMWCNT/PcCo composite can maintain long term stability, as evidenced by the optical photograph taken three months later (the inset image of Fig. 3B). Instead, part of aMWCNTs began to precipitate immediately after sonication in ethanol (the inset image of Fig. 3A). The improvement in dispersion can be attributed to the higher solubility of four peripheral isoheptyl substituents in organic solvents, which facilitates the fabrication of homogeneous electrodes. Fig. 3C and D show the TEM images of the aMWCNT/PcCo composite. Besides the distinct core and walls of carbon nanotubes, the discontinuous and irregular layer appears outside of aMWCNTs, maybe on account of the adhesion of PcCo onto the surface of aMWCNTs *via* the π–π interaction.

3.2. Electrochemical detection of AA

The electrocatalytic activity of aMWCNT/PcCo/GCE towards AA was investigated in 0.1 M PBS (pH = 7.0) at a scan rate of 10 mV s^{-1}. Fig. 4A shows the typical cyclic voltammograms (CVs) of aMWCNT/PcCo/GCE, aMWCNT/GCE, PcCo/GCE, and GCE. Obviously, the aMWCNT/PcCo/GCE generates a couple of high redox peaks in comparison with the bare GCE, aMWCNT/GCE, and PcCo/GCE. However, the pair of well-defined oxidation/reduction peaks is not observed in CVs of aMWCNT/PcCo/GCE measured in 0.1 M PBS (pH = 7.0) without AA (Fig. S2†), indicating that it is associated with the oxidation and reduction of AA. In addition, with the increase of AA concentration, the oxidation current at ~0.05 V increases linearly (as shown in Fig. S3†).

According to previous reports,[61–64] the electrocatalytic oxidation of AA on the aMWCNT/PcCo composite should undergo two steps, which could be explained by the following reaction:

$$\mathrm{PcCo(II)} \rightarrow \mathrm{PcCo(III)} + e^- \quad (1)$$

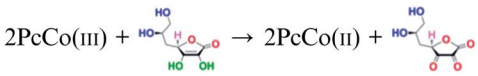

(2)

It is clear that the electrocatalytic activity of the composite highly depends on the central metal atom. However, no redox peaks are observed at PcCo/GCE (Fig. 4A), indicating that the direct electron transfer of PcCo is promoted by aMWCNTs remarkably in the composite. Meanwhile, PcCo also improves the AA detection performance of aMWCNTs due to the charge transfer between PcCo and aMWCNTs. Thus, aMWCNT/PcCo/GCE exhibits the highest oxidation current. It is important to note that the peak potential markedly shifts from 0.30 V for the bare GCE to 0.050 V for the aMWCNT/PcCo/GCE, signifying a considerable decrease (by 0.25 V) in the overpotential of AA oxidation. Compared with aMWCNT/GCE, the slight negative shift of peak potential can also be observed. The higher oxidation current and lower oxidation potential show that aMWCNT/PcCo/GCE has higher electrochemical activity than aMWCNT/GCE and bare GCE, mainly resulting from the synergistic effect between PcCo and aMWCNTs.

Fig. 4B shows the effect of the potential scan rate on the peak current for aMWCNT/PcCo/GCE, which can explore the reaction

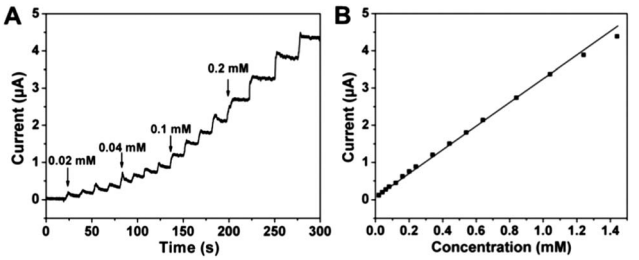

Fig. 5 (A) Amperometric response of aMWCNT/PcCo/GCE (holding at 0.050 V *vs.* SCE) to the successive addition of AA in 0.1 M PBS (pH = 7.0); (B) the calibration linear relationship of currents *versus* the AA concentration.

kinetics process. The anodic or cathodic peak currents increase linearly as the scan rate increases from 5 to 160 mV s^{-1}, but oxidation/reduction peak potentials almost remain constant (the inset image of Fig. 4B). Consequently, the linear relationship between anodic or cathodic peak currents and the scan rate is obtained, demonstrating that the electrochemical reaction of AA on aMWCNT/PcCo/GCE is a surface-controlled process.[64]

The AA sensitivity of aMWCNT/PcCo/GCE was evaluated by amperometric measurements at the optimized potential of 0.05 V. Fig. 5A shows the typical amperometric response of aMWCNT/PcCo/GCE to the successive addition of AA into the stirring 0.1 M PBS with a time interval of 25 s. Each injection of AA results in an increase of oxidation peak current. The amperometric response achieves the maximum steady-state current within 2 s, ascribing to the rapid adsorption and activation of AA on the surface of aMWCNT/PcCo/GCE, and the continuous conducting pathways of electrons.

Fig. 5B depicts a good linear relationship of currents *versus* the AA concentration in the range of 0.010 to 1.2 mM, and a current plateau is observed when the AA concentration is higher than 1.2 mM. Thus, the linear regression equation of $I_{pa} = 0.0030C_{AA} + 0.1375$, with a correlation coefficient of $R^2 = 0.9987$ ($N = 3$), is derived from the calibration curve. The AA sensor has a detection limit as low as 4.0 μM ($S/N = 3$), which is greatly superior to those of other kinds of modified electrodes for AA biosensors (as shown in ESI Table S1†). It is clear that aMWCNT/PcCo/GCE shows good AA detection performances with a lower detection limit and moderate linear range. All of the parameters indicate that aMWCNT/PcCo/GCE is very effective as a biosensor for determining AA with high activity and low overpotential.

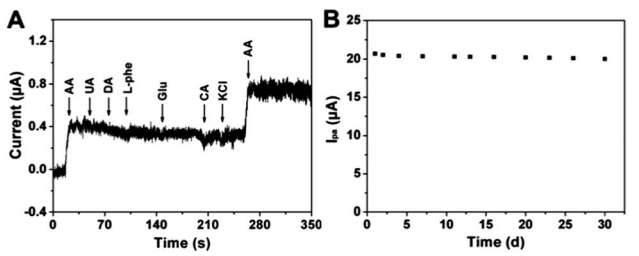

Fig. 6 (A) Amperometric response of aMWCNT/PcCo/GCE to the addition of different analytes to 35 mL of electrolyte (0.1 M PBS, pH = 7.0) at an applied potential of 0.050 V (*vs.* SCE), UA = uric acid, DA = dopamine, L-phe = L-phenylalanine, and Glu = glucose; (B) stability experiment of aMWCNT/PcCo/GCE to detect AA for 30 days.

The selectivity is one of the critical factors in practical applications. To confirm the selectivity for AA detection, interference tests were investigated by amperometric measurements. As shown in Fig. 6A, when 0.04 mM AA was added into the PBS solution, the current significantly increases with great response sensitivity. Compared with AA, the addition of several common interferents, *e.g.*, 2.5-times uric acid (UA), 2.5-times dopamine (DA), 5-times L-phenylalanine (L-phe), 25-times glucose (Glu), 25-times citric acid (CA), and 50-times KCl, in 0.1 M PBS gives a negligible current change. Nevertheless, a significant current response can also be observed for the subsequent addition of 0.04 mM of AA, indicating the high selectivity of aMWCNT/PcCo/GCE. The long-term storage stability of the aMWCNT/PcCo/GCE has also been evaluated by measuring the electrode responses at intervals of several days. The aMWCNT/PcCo/GCE retains 97.6% original current response after 30 days storage in PBS (pH = 7.0) at 4 °C (Fig. 6B). Such high stability and accuracy of aMWCNT/PcCo/GCE are acceptable for most practical applications.

4. Conclusions

In summary, the aMWCNT/PcCo composite with good dispersion was synthesized *via* noncovalent between aMWCNTs and PcCo, which is beneficial to form a uniform network-like structure on the GCE surface. Owing to the advantage of the large surface area, the continuous pathways for electron transportation, and the charge transfer between PcCo and aMWCNTs *via* the π–π stacking interaction, aMWCNT/PcCo/GCE shows outstanding properties for AA detection, such as fast response (2 s), low oxidation potential (50.0 mV), and excellent selectivity and stability.

Acknowledgements

This work was financially supported by the National Natural Science Foundation of China (51002046 and 51202061), the Natural Science Foundation for the Returned Overseas Scholars of Heilongjiang Province (LC2012C02), the Natural Science of Heilongjiang Province (B201308), the Research Fund of Heilongjiang Provincial Education Department (12511377 and 12521399), the Postdoctoral Science-Research Developmental Foundation of Heilongjiang Province (LBH-Q11015) and the Innovative Talents Program for the Returned Overseas Scholars of Harbin (2012RFLXG031).

Notes and references

1 S. Yu, C. Luo, L. Wang, H. Peng and Z. Zhu, *Analyst*, 2013, **138**, 1149–1155.
2 W. Shi, C. Liu, Y. Song, N. Lin, S. Zhou and X. Cai, *Biosens. Bioelectron.*, 2012, **38**, 100–106.
3 C.-L. Sun, C.-T. Chang, H.-H. Lee, J. G. Zhou, J. Wang, T.-K. Sham and W.-F. pong, *ACS Nano*, 2011, **5**(10), 7788–7795.

4 G. P. Keeley, A. O'Neill, N. McEvoy, N. Peltekis, J. N. Coleman and G. S. Duesberg, *J. Mater. Chem.*, 2010, **20**, 7864–7869.
5 P. B. Gai, H. J. Zhang, Y. S. Zhang, W. Liu, G. B. Zhu, X. H. Zhang and J. H. Chen, *J. Mater. Chem. B*, 2013, **1**, 2742–2749.
6 S. J. Yu, C. H. Luo, L. W. Wang, H. Peng and Z. Q. Zhu, *Analyst*, 2013, **138**, 1149–1155.
7 D. M. Fernandes, A. D. S. Barbosa, J. Pires, S. S. Balula, L. Cunha-Silva and C. Freire, *ACS Appl. Mater. Interfaces*, 2013, **5**(24), 13382–13390.
8 D. Kul, M. E. Ghica, R. Pauliukaite and C. M. A. Brett, *Talanta*, 2013, **111**, 76–84.
9 L. B. Hu, D. S. Hecht and G. Gruner, *Chem. Rev.*, 2010, **110**(10), 5790–5844.
10 P. Serp and E. Castillejos, *ChemCatChem*, 2010, **2**(1), 41–47.
11 J. M. Schnorr and T. M. Swager, *Chem. Mater.*, 2011, **23**(3), 646–657.
12 N. Saito, Y. Usui, K. Aoki, N. Narita, M. Shimizu, K. Hara, N. Ogiwara, K. Nakamura, N. Ishigaki, H. Kato, S. Taruta and M. Endo, *Chem. Soc. Rev.*, 2009, **38**(7), 1897–1903.
13 G. Lota, K. Fic and E. Frackowiak, *Energy Environ. Sci.*, 2011, **4**(5), 1592–1605.
14 L. Zhou, J.-P. Wang, L. Gai, D.-J. Li and Y.-B. Li, *Sens. Actuators, B*, 2013, **181**, 65–70.
15 W. Grosse, J. Champavert, S. Gambhir, G. G. Wallace and S. E. Moulton, *Carbon*, 2013, **61**, 467–475.
16 P. Li, H. L. Liu, J. Yang, D. M. Sun, Y. Chen, Y. M. Zhou, C. X. Cai and T. H. Lu, *J. Mater. Chem. B*, 2014, **2**(1), 102–109.
17 C. Han, A. Doepke, W. Cho, V. Likodimos, A. A. de la Cruz, T. Back, W. R. Heineman, H. B. Halsall, V. N. Shanov, M. J. Schulz, P. Falaras and D. D. Dionysiou, *Adv. Funct. Mater.*, 2013, **23**(14), 1807–1816.
18 X. Zhao, Y. Liu, J. Lu, J. H. Zhou and J. H. Li, *Chem.–Eur. J.*, 2012, **18**(12), 3687–3694.
19 N. Karousis, N. Tagmatarchis and D. Tasis, *Chem. Rev.*, 2010, **110**(9), 5366–5397.
20 X. H. Peng and S. S. Wong, *Adv. Mater.*, 2009, **21**(6), 625–642.
21 B. I. Kharisov, O. V. Kharissova, H. L. Gutierrez and U. O. Mendez, *Ind. Eng. Chem. Res.*, 2009, **48**(2), 572–590.
22 M. N. Ding, Y. F. Tang, P. P. Gou, M. J. Reber and A. Star, *Adv. Mater.*, 2011, **23**(4), 536–540.
23 N. He, Y. Chen, J. R. Bai, J. Wang, W. J. Blau and J. H. Zhu, *J. Phys. Chem. C*, 2009, **113**(30), 13029–13035.
24 M.-Y. Hua, Y.-C. Lin, R.-Y. Tsai and H.-C. Chen, *J. Mater. Chem.*, 2012, **22**(6), 2566–2574.
25 J. Bartelmess, B. Ballesteros, G. de la Torre, D. Kiessling, S. Campidelli, M. Prato, T. Torres and D. M. Guldi, *J. Am. Chem. Soc.*, 2010, **132**(45), 16202–16211.
26 W. W. Tu, J. P. Lei, G. Q. Jian, Z. Hu and H. X. Ju, *Chem.–Eur. J.*, 2010, **16**(13), 4120–4126.
27 X. L. Li, Y. J. Qin, S. T. Picraux and Z.-X. Guo, *J. Mater. Chem.*, 2011, **21**(21), 7527–7547.
28 J. K. Sprafke, S. D. Stranks, J. H. Warner, R. J. Nicholas and H. L. Anderson, *Angew. Chem., Int. Ed.*, 2011, **50**(10), 2313–2316.
29 C. M. Yap, G. Q. Xu and S. G. Ang, *Anal. Chem.*, 2013, **85**(1), 107–113.
30 A. Sengul, H. Z. Dogan, A. Altindal, A. R. Ozkaya, B. Salih and O. Bekaroglu, *Dalton Trans.*, 2012, **41**(25), 7559–7572.
31 W. M. Li, A. P. Yu, D. C. Higgins, B. G. Llanos and Z. W. Chen, *J. Am. Chem. Soc.*, 2010, **132**(48), 17056–17058.
32 T. Honda, T. Kojima and S. Fukuzumi, *J. Am. Chem. Soc.*, 2012, **134**(9), 4196–4206.
33 K. Wang, L. N. Dai, Q. Liu, H. N. Li, C. Ju, J. Wu and H. M. Li, *Analyst*, 2011, **136**(20), 4344–4349.
34 A. J. Jeevagan and S. A. John, *RSC Adv.*, 2013, **3**(7), 2256–2264.
35 S. B. A. Barros, A. Rahim, A. A. Tanaka, L. T. Arenas, R. Landers and Y. Gushikem, *Electrochim. Acta*, 2013, **87**, 140–147.
36 F. D'Souza and O. Ito, *Chem. Commun.*, 2009, 4913–4928.
37 G. Bottari, O. Trukhina, M. Ince and T. Torres, *Coord. Chem. Rev.*, 2012, **256**(21–22), 2453–2477.
38 J. Bartelmess, C. Ehli, J.-J. Cid, M. Garcia-Iglesias, P. Vazquez, T. Torres and D. M. Guldi, *Chem. Sci.*, 2011, **2**(4), 652–660.
39 R. G. Cao, R. Thapa, H. Kim, X. D. Xu, M. G. Kim, Q. Li, N. Park, M. L. Liu and J. Cho, *Nat. Commun.*, 2013, **4**, 2076.
40 J. Bartelmess, C. Ehli, J.-J. Cid, M. Garcia-Iglesias, P. Vazquez, T. Torres and D. M. Guldi, *J. Mater. Chem.*, 2011, **21**(22), 8014–8020.
41 A. Abbaspour and E. Mirahmadi, *Electrochim. Acta*, 2013, **105**, 92–98.
42 A. G. Porras-Gutierrez, B. A. Frontana-Uribe, S. Gutierrez-Granados, S. Griveau and F. Bedioui, *Electrochim. Acta*, 2013, **89**, 840–847.
43 X. Sun, F. L. Li, G. H. Shen, J. D. Huang and X. Y. Wang, *Analyst*, 2014, **139**(1), 299–308.
44 F. C. Moraes, L. H. Mascaro, S. A. S. Machado and C. M. A. Brett, *Electroanalysis*, 2010, **22**(14), 1586–1591.
45 I. M. Apetrei, M. L. Rodriguez-Mendez, C. Apetrei and J. A. de Saja, *Sens. Actuators, B*, 2013, **177**, 138–144.
46 A. T. Chidembo, K. I. Ozoemena, B. O. Agboola, V. Gupta, G. G. Wildgoose and R. G. Compton, *Energy Environ. Sci.*, 2010, **3**(2), 228–236.
47 T. Mugadza and T. Nyokong, *Electrochim. Acta*, 2010, **55**(20), 6049–6057.
48 H. Z. Zhao, Y. Zhang, B. Zhao, Y. Y. Chang and Z. S. Li, *Environ. Sci. Technol.*, 2012, **46**(9), 5198–5204.
49 P. Mashazi, T. Mugadza, N. Sosibo, P. Mdluli, S. Vilakazi and T. Nyokong, *Talanta*, 2011, **85**(4), 2202–2211.
50 Y. Zhang, R. Yuan, Y. Q. Chai, X. Zhong and H. A. Zhong, *Talanta*, 2006, **70**(3), 588–594.
51 A. P. Gutierrez, S. Griveau, C. Richard, A. Pailleret, S. G. Granados and F. Bedioui, *Electroanalysis*, 2009, **21**(21), 2303–2310.
52 J. F. Silva, S. Griveau, C. Richard, J. H. Zagal and F. Bedioui, *Electrochem. Commun.*, 2007, **9**(7), 1629–1634.
53 X. J. Wang, X. Chen, D. G. Evans and W. S. Yang, *Sens. Actuators, B*, 2011, **160**(1), 1444–1449.
54 X. Chen, X. M. Hu, L. An, N. L. Zhang, D. G. Xia, X. Zuo and X. Y. Wang, *Electroanalysis*, 2014, **5**(1), 68–74.
55 Y. Yamada, S. Yoshida, T. Honda and S. Fukuzumi, *Energy Environ. Sci.*, 2011, **4**(8), 2822–2825.

56 H. J. Li, Z. W. Xu, K. Z. Li, X. H. Hou, G. X. Cao, Q. L. Zhang and Z. Y. Cao, *J. Mater. Chem.*, 2011, **21**(4), 1181–1186.
57 P. Li, Y. Ding, A. Wang, L. Zhou, S. Wei, Y. M. Zhou, Y. W. Tang, Y. Chen, C. X. Cai and T. H. Lu, *ACS Appl. Mater. Interfaces*, 2013, **5**, 2255–2260.
58 L. Liao, Q. Zhang, Z. Su, Z. Zhao, Y. Wang, Y. Li, X. Lu, D. Wei, G. Feng, Q. Yu, X. Cai, J. Zhao, Z. Ren, H. Fang, F. Robles-Hernandez, S. Baldelli and J. Bao, *Nat. Nanotechnol.*, 2014, **9**, 69–73.
59 W. Lu, N. Li, W. Chen and Y. Yao, *Carbon*, 2009, **47**, 3337–3345.
60 Y. Y. Wang, N. T. Hu, Z. H. Zhou, X. Dong, Z. Wang, Z. Yang, H. Wei, E. S.-W. Kong and Y. F. Zhang, *J. Mater. Chem.*, 2011, **21**, 3779–3787.
61 X. Zuo, H. Zhang and N. Li, *Sens. Actuators, B*, 2012, **161**, 1074–1079.
62 C.-Y. Lin, A. Balamurugan, Y.-H. Lai and K.-C. Ho, *Talanta*, 2010, **82**, 1905–1911.
63 L. Y. Zhao, K. Liao, M. Pynenburg, L. Wong, N. Heining, J. P. Thomas and K. T. Leung, *ACS Appl. Mater. Interfaces*, 2013, **5**, 2410–2416.
64 A. J. Jeevagan and S. A. John, *Bioelectrochemistry*, 2012, **85**, 50–55.